This article was downloaded by: [Umberto Marini Bettolo Marconi]
On: 16 October 2014, At: 03:36
Publisher: Taylor & Francis
Informa Ltd Registered in England and Wales Registered Number: 1072954 Registered office: Mortimer House, 37-41 Mortimer Street, London W1T 3JH, UK

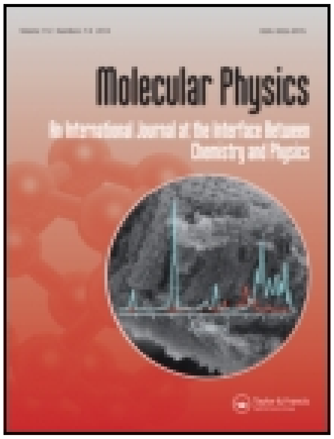

Molecular Physics: An International Journal at the Interface Between Chemistry and Physics
Publication details, including instructions for authors and subscription information:
http://www.tandfonline.com/loi/tmph20

Ionic conduction in non-uniform nanopores and DNA translocation: a Nernst-Planck-Jacobs one-dimensional description

Umberto Marini Bettolo Marconi[a] & Simone Melchionna[b]
[a] Scuola di Scienze e Tecnologie, Università di Camerino, Camerino, Italy
[b] CNR-IPCF, Consiglio Nazionale delle Ricerche, Dipartimento di Fisica, Università Sapienza, Roma, Italy

Published online: 01 Nov 2013.

To cite this article: Umberto Marini Bettolo Marconi & Simone Melchionna (2013) Ionic conduction in non-uniform nanopores and DNA translocation: a Nernst-Planck-Jacobs one-dimensional description, Molecular Physics: An International Journal at the Interface Between Chemistry and Physics, 111:22-23, 3493-3501, DOI: 10.1080/00268976.2013.826828

To link to this article: http://dx.doi.org/10.1080/00268976.2013.826828

PLEASE SCROLL DOWN FOR ARTICLE

Taylor & Francis makes every effort to ensure the accuracy of all the information (the “Content”) contained in the publications on our platform. However, Taylor & Francis, our agents, and our licensors make no representations or warranties whatsoever as to the accuracy, completeness, or suitability for any purpose of the Content. Any opinions and views expressed in this publication are the opinions and views of the authors, and are not the views of or endorsed by Taylor & Francis. The accuracy of the Content should not be relied upon and should be independently verified with primary sources of information. Taylor and Francis shall not be liable for any losses, actions, claims, proceedings, demands, costs, expenses, damages, and other liabilities whatsoever or howsoever caused arising directly or indirectly in connection with, in relation to or arising out of the use of the Content.

This article may be used for research, teaching, and private study purposes. Any substantial or systematic reproduction, redistribution, reselling, loan, sub-licensing, systematic supply, or distribution in any form to anyone is expressly forbidden. Terms & Conditions of access and use can be found at http://www.tandfonline.com/page/terms-and-conditions

Molecular Physics, 2013
Vol. 111, Nos. 22–23, 3493–3501, http://dx.doi.org/10.1080/00268976.2013.826828

INVITED ARTICLE

Ionic conduction in non-uniform nanopores and DNA translocation: a Nernst–Planck–Jacobs one-dimensional description

Umberto Marini Bettolo Marconi[a,*] and Simone Melchionna[b]

[a]*Scuola di Scienze e Tecnologie, Università di Camerino, Camerino, Italy;* [b]*CNR-IPCF, Consiglio Nazionale delle Ricerche, Dipartimento di Fisica, Università Sapienza, Roma, Italy*

(*Received 11 June 2013; accepted 16 July 2013*)

The conduction of an electrolyte solution in the presence of a DNA intruder in a synthetic charged pore is studied by theoretical means. The pore conductivity is controlled by two competing mechanisms: the steric effect of the DNA decreases the current and the extra-surface charges determine an increase in the number of charge carriers that increase the current. By using a Nernst–Planck description of the electrolyte and a one-dimensional advection-diffusion equation similar to the Jacobs–Zwanzig method, we obtain the characteristic curve within the local electroneutrality approximation. Such an information allows predicting the variation of the conductance caused by the DNA intruder and determining the current blockage/enhancement phase diagram.

Keywords: ionic conduction; DNA translocation; nanopores; electrodiffusion

1. Introduction

In the last few years, we have witnessed a huge activity in the area termed nanofluidics whose applications range from the construction of nanofluidic diodes, rectifying properties, energy conversion, to biological ion channels, molecule delivery and sensing [1–5]. Understanding the physical mechanisms of ion transport in nanometre-sized channels is of capital importance in order to develop efficient techniques to detect and manipulate single biomolecules, which are electrically charged in most cases of interest.

Nanochannels may provide selectivity to charged ions and molecules, such as DNA, due to the presence of unscreened surface charges at their walls. At distances less than 100 nm and submolar electrolyte concentrations, electrostatic screening may not be effective so that the surface charges repel the co-ions and favour the passage of counterions. In this regime, the conduction of electric charges is governed by the surface charge and the effect of the electro-osmosis, that is, the charge motion induced by the presence of double layers near the walls, is always smaller than the electrophoretic effect, although not always negligible [6].

When analysing the system and neglecting electro-osmotic effects, the starting point is the three-dimensional (3D) Poisson–Nernst–Planck (PNP) equation describing the drift-diffusion of ions in liquid solutions under the influence of an electric driving field [7]. If this transport process occurs in very narrow long pores, it is convenient to consider a reduced description, where the important properties of the system are expressed in terms of a one-dimensional effective PNP equation. This is achieved by means of a homogenisation technique, which leads to a set of coupled one-dimensional equations for the sectional averages of the ionic concentrations and electric field. The method can also handle channel inhomogeneities such as narrowings and/or non uniformities in the chemical nature of their confining surfaces. The idea goes back to Jacobs [8] who proposed an effective one-dimensional representation of the diffusion equation for channels of non-uniform section. His work was continued by Zwanzig [9] and other authors [10–13], who used the concept of entropic barriers. In the study of ion channels, the same homogenisation techniques has also been applied [14].

The resulting one-dimensional PNP model consists of two diffusion equations for the species densities in the presence of the self-consistent electric potential. Such a potential is the solution of a Poisson problem whose source is the instantaneous charge distribution. The equation is highly non local and thus requires a numerical solution [15]. A much faster solution is however possible in the high electrolyte concentration regime, because the Debye screening length is small compared to the typical dimensions of the system under scrutiny. It is therefore possible to replace the PNP equation by the simpler Nernst–Planck equation in conjunction with the local electroneutrality (LEN) condition, which gives a local relation between the potential and the charge distribution. Many authors have used this classical approximation [2,7,16–19], originally introduced by Planck, to obtain simple descriptions of the solute

---

*Corresponding author. Email: umberto.marinibettolo@unicam.it distribution and derive the current–voltage characteristic curve. The method has been validated in a recent paper compared to 3D simulations [20].

In the present paper, we apply the Nernst–Planck equation in the LEN approximation to derive the characteristic curve for a model of pore with an access region modelled as a funnel. We also consider how the pore resistance changes with the diameter of the inner part and with the surface charge and the presence of a cylindrical intruder modelling a DNA molecule.

2. Nernst–Planck equation in the LEN approximation

2.1. *Model*

In this section, we describe a simple model to predict the change in conductivity due to the presence of double-stranded DNA in a pore, by extending the methods introduced elsewhere to a system of coaxial cylinders [20]. A DNA molecule is assimilated to a very long thin cylindrical of radius R_i and the pore is modelled by two funnels joined by a cylindrical section with $R_w(x) > R_i$ (Figure 1). Such model has been shown to be an accurate representation of double-stranded DNA in nanopores [21]. By this approach, we account for two separate effects: (1) the reduced space available to the ionic solution due to the presence of the DNA molecule and (2) the extra contribution due to the mobile charges brought about by the DNA surface charge. Effect (1) tends to increase the resistance of the system, whereas effect (2) tends to decrease it.

We consider a nanochannel comprises three sections: an entrance and an exit region modelled as conical funnels joined together by a straight cylindrical sector of radius R_w. On the inner walls of the cylindrical section sits a charge of surface density Σ_w. At each end of the system, the charge concentration of the electrolyte is fixed to the bulk value, associated to two bulk reservoirs. We also model a cylindrical intruder, coaxial with the first cylinder, of fixed radius $R_i < R_w$ and carrying a surface charge Σ_i. An electrolyte solution can flow in the cavity formed by the two subsystems.

A standard approach to the investigation of the electrophoretic transport is provided by the PNP model. One considers the continuity equation for each ionic species α present in solution,

$$\frac{\partial n^\alpha(\mathbf{r},t)}{\partial t} + \nabla\cdot\mathbf{J}^\alpha(\mathbf{r},t) = 0 \tag{1}$$

supplemented by the following constitutive equations for the partial currents $\mathbf{J}^\alpha$,

$$\mathbf{J}^\alpha(\mathbf{r},t) = -D^\alpha\left(\nabla n^\alpha(\mathbf{r},t) - \frac{ez^\alpha n^\alpha(\mathbf{r},t)}{k_BT}\mathbf{E}(\mathbf{r},t)\right) \tag{2}$$

where D^α is the diffusion coefficient of each species, e is the elementary charge, z^α is the ionic valence, while the electric field $\mathbf{E} = -\nabla V$, where V is the electric potential, is obtained from the charge distribution using the Poisson equation,

$$\nabla\cdot\mathbf{E}(\mathbf{r},t) = \frac{ze}{\epsilon}\left(n^+(\mathbf{r},t) - n^-(\mathbf{r},t)\right). \tag{3}$$

2.2. *Effective one-dimensional problem*

If the motion of the ions occurs in very narrow cylindrical channels, using the dominance of the motions along the axial direction, it is possible to deduce the following one-dimensional equation [20],

$$\frac{\partial c^\alpha(x,t)}{\partial t} = D^\alpha\frac{\partial}{\partial x}\left(\frac{\partial c^\alpha(x,t)}{\partial x} - \frac{\partial \ln S(x)}{\partial x}c^\alpha(x,t) - \frac{ez^\alpha\langle E(x,t)\rangle}{k_BT}c^\alpha(x,t)\right), \tag{4}$$

where $c^\alpha(x,t)$ is related to the sectionally averaged density,

$$< n^\alpha(x,t) >\equiv \frac{1}{S(x)}\int_{S(x)} dS\, n^\alpha(\mathbf{r},t), \tag{5}$$

by $c^\alpha(x,\ t) = <n^\alpha(x,\ t)> S(x)$, and $S(x)$ is the section of the space between the cylinders or between the inner cylinder and the funnels, at the axial position x. In addition, $\langle E(x,t)\rangle \equiv \frac{1}{S(x)}\int_{S(x)} dS\, E_x(\mathbf{r},t)$.

Due to the impermeability of the lateral boundaries, the normal component of the current of each species vanishes at the walls,

$$\mathbf{J}^\alpha(\mathbf{r},\mathbf{t})\cdot\mathbf{n}|_S = 0. \tag{6}$$

By restricting the discussion to the stationary regime, $\frac{\partial n^\alpha(\mathbf{r},t)}{\partial t} = 0$, the divergence of each current must vanish

$$\nabla\cdot\mathbf{J}^\alpha(\mathbf{r}) = 0, \tag{7}$$

and one finds that $\frac{d}{dx}\left(\frac{\langle J_x^\alpha(x)\rangle}{D^\alpha}S(x)\right) = 0$, where $\langle J^\alpha(x)\rangle \equiv \frac{1}{S(x)}\int_{S(x)} dS\, J_x^\alpha(\mathbf{r},t)$, so that the flux in the axial direction is constant,

$$I^\alpha = \frac{\langle J^\alpha(x)\rangle}{D^\alpha}S(x) = \text{const.} \tag{8}$$

We use this result to write down the following ordinary first-order differential equations for the stationary case,

$$\frac{dc^\alpha(x)}{dx} - \frac{d\ln S(x)}{dx}c^\alpha(x,t) - \frac{ez^\alpha\langle E(x)\rangle}{k_BT}c^\alpha(x) = -I^\alpha. \tag{9}$$

The solution of Equation (9) is

$$c^{\pm}(x) = c^{\pm}(0)\frac{S(x)}{S(0)}e^{\mp\phi(x)} - I^{\pm}e^{\mp\phi(x)}S(x) \times \int_0^x dx' e^{\pm\phi(x')}\frac{1}{S(x')} \tag{10}$$

with

$$\phi(x) = -\frac{e}{k_B T}\int_0^x dx' \langle E(x')\rangle \,. \tag{11}$$

The equation for c^{α} must be supplemented by the equation for the axial component of the sectionally averaged electric field, $\langle E(x)\rangle$, which fulfils the following equation:

$$\frac{d\langle E(x)\rangle}{dx} + \frac{d\ln S(x)}{dx}\langle E(x)\rangle = \frac{1}{\epsilon S(x)}\left[z^+c^+(x) + z^-c^-(x) + 2\pi R_w(x)\Sigma_w(x) \times \sqrt{1+\left(\frac{dR_w(x)}{dx}\right)^2} + 2\pi R_i\Sigma_i\right], \tag{12}$$

where the last two terms in Equation (12) have been obtained using the relation between the electric field normal to the surface and the surface charge to eliminate the radial component **E** [20]. As a result, the surface charge appears explicitly as a source term in Equation (12).

We notice that Equations (9) and (12) can be generalised to the case of an arbitrary distribution of radii of co-axial cylindrical objects. Let us consider a sequence of K radial profiles $R_{\alpha}(x)$, with $R_{\alpha}(x) > R_{\alpha+1}(x)$, in a system with a maximal available section πR_0^2, taken to be constant. The available section is $S(x) = \pi\sum_{\alpha=0}^{K}(-1)^{\alpha}R_{\alpha}^2$, subjected to the condition $S(x) > 0$. For each profile R_{α}, we associate a profile for the number of charges per unit area $\Sigma_{\alpha}(x)$. Then, Equation (9) remains valid and Equation (12) generalises to

$$\frac{d\langle E(x)\rangle}{dx} + \frac{d\ln S(x)}{dx}\langle E(x)\rangle = \frac{1}{\epsilon S(x)}\left[z^+c^+(x) + z^-c^-(x) + 2\pi\sum_{\alpha=1}^{K}R_{\alpha}(x)\Sigma_{\alpha}(x) \times \sqrt{1+\left(\frac{dR_{\alpha}(x)}{dx}\right)^2}\right]. \tag{13}$$

In the present study, we particularise to $S(x) \equiv \pi(R_w^2(x) - R_i^2)$. Few comments are in order: the presence of the square root stems from the fact that the surface area of the walls is proportional to the length of the line described by the curve $R_w(x)$; finally the second term on the left-hand side, due to the sectional averaging, has the form predicted by [22] and enforces the flux conservation of the electric field in the absence of sources (see [20] for details).

Summarising, in the case of a binary electrolyte it is necessary to solve a system of three coupled equations for the ions and the electric field, namely Equation (4) for time-dependent conditions, or Equation (9) for stationary conditions, and Equation (12). In some applications, it is however possible to employ approximations that avoid the solution of the highly non-local Poisson equation.

In the literature, the main approaches to study transport in charged pores are of two kinds and valid in two different regimes: (1) when the pores are short with respect to the Debye screening length, this is the Goldman approximation that assumes the axial component of the electric field constant along the pore and (2) in the case where λ_D is much smaller than the typical length of the channels one can employ the LEN approximation. In practice, instead of solving the Poisson equation for the electrostatic potential, one determines an effective potential ϕ, which enforces the LEN. This is achieved for electrolyte solutions of moderate concentrations on a scale, which is somehow larger than the atomic scale, therefore the LEN conditions hold true in a coarse-grained sense. In the following, we will discuss these approximations in detail.

For the sake of simplicity, we assume a binary electrolyte with valences $z^- = -z^+ = 1$. To establish these two very common approximations, it is useful to consider the following non-dimensional variables in Equation (12): $\tilde{E} \equiv \frac{zeL}{k_B T}\langle E(x)\rangle$ and $\tilde{x} = x/L$, where L is the longitudinal size of the channel of interest [23]. Let us assume R_0 to be typical transversal size of the channel, πR_w^2 to be its section and c_b to be the bulk value of $c^{\pm}$, $\tilde{c}^{\pm} \equiv \frac{c^{\pm}}{c_b}$ and $\tilde{R}(\tilde{x}) \equiv \frac{R_w(x)}{R_0}$. Thus, we rewrite Equation (12) as

$$\frac{d\tilde{E}(\tilde{x})}{d\tilde{x}} + \frac{2}{\tilde{R}(\tilde{x})}\frac{d\tilde{R}(\tilde{x})}{d\tilde{x}}\tilde{E}(\tilde{x}) = \frac{L^2}{\lambda_C^2\pi\tilde{R}^2(\tilde{x})}\left[\sum_{\alpha}z^{\alpha}\tilde{c}^{\alpha}(\tilde{x}) + 2\pi\tilde{R}(\tilde{x})\tilde{\Sigma}(\tilde{x}) \times \sqrt{1+\left(\frac{R_0}{L}\frac{d\tilde{R}(\tilde{x})}{d\tilde{x}}\right)^2} + 2\pi\frac{R_i}{R_0}\Sigma_i\right], \tag{14}$$

where $\lambda_C = \sqrt{\frac{\epsilon k_B T}{(ze)^2}\frac{\pi R_0^2}{2c_b}}$ is a local screening length associated with the channel and $\tilde{\Sigma} \equiv \Sigma R_0/2c_b$. The first important limit occurs when $\lambda_C/L \to 0$, which gives the condition,

$$z(c^+(x) - c^-(x)) + 2\pi R_w(x)\Sigma_{\mathrm{wall}}(x)\sqrt{1+\left(\frac{dR_w(x)}{dx}\right)^2} + 2\pi R_i\Sigma_i = 0, \tag{15}$$

the celebrated LEN condition that replaces the Poisson equation by a much simpler constraint on the partial densities [7].

The opposite limit, $\lambda_C/L \to \infty$, often considered in membrane science, implies the condition of conservation of the flux of the electric field in a tube of varying section, that is, $E(x)R^2(x) =$ constant. Notice that in the case of constant section, it reduces to the constant field approximation introduced by Goldman in 1943 and Hodkin–Goldman–Katz, forming the basis of the theory of thin membranes [24].

The LEN approximation is widely employed in the description of electrolytic transport due to its relative simplicity. Its main advantage is that for the two component electrolyte at steady state, one can eliminate the charge-density distribution in favour of the fixed surface charge distribution and solve a very simple equation for the density profiles in terms of the electric current and the mass current. Piecewise constant surface charge distributions can be easily accounted for and it is possible to determine the matching conditions for the density and the potential at the junctures. The numerical solutions allow us to compute numerically the conductance of channels of different shapes through the I–V relation. They also allow to compute the selectivity of a channel defined as the ratio between the current due to the two species. The present method based on LEN is a simple extension of the one proposed to discuss the properties of nanofluidic diodes [1]. To the best of our knowledge, the Nernst–Planck equations under the LEN approximation, for which there exist many applications in the case of uniform pores, have not been considered in the presence of channels of non-uniform shapes.

Hereafter, we derive the consequences of the LEN condition by first introducing new concentration variables,

$$c_N(x) = c^+(x) + c^-(x) \tag{16}$$

$$c_Q(x) = c^+(x) - c^-(x), \tag{17}$$

and currents

$$I_N = (I^+ + I^-) \tag{18}$$

$$I_Q = (I^+ - I^-), \tag{19}$$

and we rewrite the Nernst–Planck equations (9) as

$$\frac{dc_N(x)}{dx} - \frac{d\ln S(x)}{dx} c_N(x) + \phi'(x) c_Q(x) = -I_N \tag{20}$$

$$\frac{dc_Q(x)}{dx} - \frac{d\ln S(x)}{dx} c_Q(x) + \phi'(x) c_N(x) = -I_Q. \tag{21}$$

Since the LEN condition (Equation (15)) dictates that the charge density obeys the following condition:

$$c_Q(x) = -\left[2\pi R_w(x)\Sigma_{\rm wall}(x)\sqrt{1+\left(\frac{dR_w(x)}{dx}\right)^2} + 2\pi R_i \Sigma_i\right], \tag{22}$$

we use Equation (21) to determine the potential $\phi(x)$. Finally, $c_Q(x)$ and $\phi(x)$ are inserted in Equation (20) to determine the concentration $c_N(x)$.

Coherently with the limit $\lambda_C/L \to 0$, we assume that regions of different surface charge are separated by very thin interfaces. At each of these interface one has to apply the appropriate juncture conditions for the concentrations and the potential. A convenient modelling is to employ a piecewise constant surface charge distribution, $\Sigma(x)$. To derive the juncture conditions, we integrate the resulting equations using Equation (10) across a juncture,

$$\begin{aligned}\frac{c^\pm(x+\delta)}{S(x+\delta)} = \frac{c^\pm(x-\delta)}{S(x-\delta)}\frac{\exp(\mp(\phi(x+\delta))}{\exp(\mp\phi(x-\delta))} \\ - \exp(\mp\phi(x+\delta))\int_{x-\delta}^{x+\delta} dx' \exp(\pm\phi(x')) \\ \times \frac{I_x^\pm(x')}{S(x').}\end{aligned} \tag{23}$$

When the thickness of the boundary region $\delta \propto \lambda_C \to 0$, the integral vanishes and we obtain

$$\frac{c^+(x+\delta)c^-(x+\delta)}{S^2(x+\delta)} = \frac{c^+(x-\delta)c^-(x-\delta)}{S^2(x-\delta)} \tag{24}$$

and

$$\begin{aligned}\Delta\phi &= \phi(x+\delta) - \phi(x-\delta) \\ &= \frac{1}{2}\ln\left(\frac{c^-(x+\delta)}{c^+(x+\delta)}\frac{c^+(x-\delta)}{c^-(x-\delta)}\right).\end{aligned} \tag{25}$$

Using the LEN condition Equation (15), we relate the mass concentration per unit length on the two sides of the boundary,

$$\frac{c_N^2(x+\delta) - c_Q^2(x+\delta)}{S^2(x+\delta)} = \frac{c_N^2(x-\delta) - c_Q^2(x-\delta)}{S^2(x-\delta)}. \tag{26}$$

Equations (24)–(26) can be viewed as a generalisation of the standard Donnan relations [25,26] between the densities and the potentials of two adjacent regions having different ionic concentrations and/or different surface charges. To this purpose, we notice that by setting $c^+(x-\delta) = c^-(x-\delta) = c_{\rm bulk}$ one immediately recovers the well-known relation $\Delta\phi = \frac{1}{2}\ln(\frac{c^-(x+\delta)}{c^+(x+\delta)})$ giving the value of the Donnan potential [26] resulting from the asymmetric distribution of the charged species within the pore. Conditions (24)–(26) together with Equation (20) can be used to derive the properties of pores of non-uniform section and non-uniform charge.

Utilising such an approximation, it is possible to derive numerical solutions under the form of simple recursive relations for the reduced concentration c_N and for the potential ϕ, at some specific grid point without solving the Poisson equation. In practice, one computes the profile $c_N(x)$ for fixed values of the charge and density current and I_Q and I_N for a given piecewise constant charge–density distribution c_Q. The value of I_N is determined using a shooting method as to satisfy the boundary condition $c_N(L) = c_{\text{out}}$. Since the value of V depends on the electric current I_Q, one obtains the *I*-*V* characteristic curve of the system.

2.3. Resistance

We discuss an important characteristic of a channel, namely its electrical conductance in the case of channels of varying section. Variations in the ionic conductance upon the insertion of a biological molecule in a nanopore are in fact currently investigated as a tool for detecting and sequencing DNA molecules [27]. Interpretative models describing the pores as cylindrical channels fail to describe the correct dependence of the conductance on the pore width and one has to include the region adjacent to the pore ends, which is known to contribute to the conductance with the so-called access conductance [28,29].

In the present modelling, we assimilate the two reservoir chambers to two conical sections whose smallest radius is R_0 and $R_w(x) = R_0 \pm B_0(x - x_{I,O})$ with $B =$ the slope of the funnel and $x_{I,O}$ are the coordinates of the inlet and of the outlet, respectively, of the cylindrical section joining the chambers.

With the help of Equation (21), we derive the expression for the resistance of a wire. For this purpose, we assume that both the surface charge and the mass current, I_N, vanish. By assuming that the charge carriers have a nearly uniform volume distribution, i.e. $c_N(x)/S(x) \simeq 2n_s$, where n_s is the bulk density of one species of ions, we obtain

$$V(x_O) - V(x_I) = -\frac{k_BT}{ze}\frac{I_Q}{2n_s}\int_{x_I}^{x_O} dx\,\frac{1}{S(x)}. \tag{27}$$

For the cylindrical region of the pore of length L and constant radius R_0, the resistance is

$$\mathcal{R}_{\text{ch}} = \rho_0\frac{L}{\pi(R_0^2 - R_i^2)}, \tag{28}$$

where ρ_0 is the specific resistivity, related to the microscopic parameters by $\rho_0 = \frac{k_BT}{D}\frac{1}{2n_se^2}$. In the limit $R_w(x_O)/R_0 \gg 1$, the funnel resistance is

$$\mathcal{R}_{\text{funnel}} = \frac{\rho_0}{\pi}\frac{1}{2B_0R_i}\ln\left(\frac{1+\frac{R_i}{R_0}}{1-\frac{R_i}{R_0}}\right), \tag{29}$$

which reduces to the value $\mathcal{R}_{\text{funnel}} \simeq \rho_0\frac{1}{\pi B_0}\frac{1}{R_0}$ when the radius of the intruder vanishes. The total resistance of the channel is $\mathcal{R}_{\text{total}} = \mathcal{R}_{\text{ch}} + 2\mathcal{R}_{\text{funnel}}$, and for large values of R_0 this is dominated by the funnels, the so-called access resistance. The total conductance of an open pore (i.e. without the intruder), reads

$$G(R_0) = \frac{\pi}{\rho_0}\frac{1}{\frac{L}{R_0^2} + \frac{2}{B_0}\frac{1}{R_0}}. \tag{30}$$

Notice that the behaviour described by Equation (30) is purely Ohmic and differs by a constant geometrical prefactor from the formula proposed by Dekker *et al.*, who considered an hourglass-shaped pore [27]. Both the access resistance and the pore resistance increase due to the reduced effective section of the pore caused by the finiteness of intruder radius R_i. With the help of Equation (27) we compute, in the limit of short pores $R_0/L \gg 1$, the difference between the conductances of the open pore and the pore with the intruder and assuming $R_i < R_0$ we obtain

$$\Delta G = G(R_0) - G\left(\sqrt{R_0^2 - R_i^2}\right) \approx \frac{\pi B_0}{6}\frac{R_i^2}{\rho_0 R_0} \tag{31}$$

that can be compared with Dekker's phenomenological formula [27],

$$\Delta G_{\text{Dekker}} = G_{\text{Dekker}}(R_0) - G_{\text{Dekker}}\left(\sqrt{R_0^2 - R_i^2}\right) \approx \frac{1}{2}\frac{R_i^2}{\rho_0 R_0} \tag{32}$$

obtained by replacing the conductance in Equation (30) by the following expression:

$$G_{\text{Dekker}}(R_0) = \frac{\pi}{\rho_0}\frac{1}{\frac{L}{R_0^2} + \frac{\pi}{2R_0}}, \tag{33}$$

based on a different estimate of the access resistance. In both approaches, the presence of the intruder determines a decrease of the effective pore section and consequently of the relative pore conductance, G_i, so that $G_i < G_{\text{open}}$ for purely steric reasons. In the case of long pores, $R_0/L \ll 1$ that represents the typical experimental condition, we obtain instead $\Delta G \simeq \frac{\pi}{\rho_0}\frac{1}{L}R_i^2$. The case studied numerically in the following belongs to the latter regime.

From the equations, it is apparent that the presence of DNA results in an increase i the pore conductance [4].

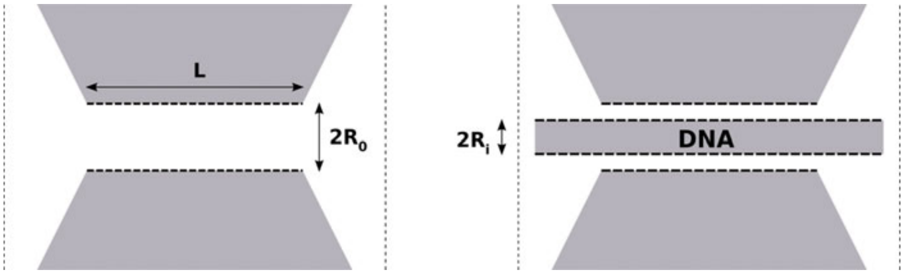

Figure 1. Sketch of the systems. Left: Channel without DNA intruder. Right: Channel with DNA intruder. The horizontal dashed lines represent the regions where the surface charge density is present, while the vertical lines represent the boundaries of the system where the electric potential is imposed.

The DNA charge determines an increase in the number of mobile charge carriers due to the LEN condition, an effect which can be quite relevant in the case of moderately dilute solutions and small pore radii, comparable in size with the DNA effective radius. We describe the presence of the non-uniform surface charge (for not too large values of Σ_w, or for not too dilute solutions), by modifying the local carrier density within the channel, changes from the bare value $2n_s$ to a new value $2n_s^*$, which depends on the position within the pore given by

$$n_s^*(x) = \sqrt{n_s^2 + \left(\frac{\Sigma_w(x)R_w(x) + \Sigma_i R_i}{R_w^2(x) - R_i^2}\right)^2}. \tag{34}$$

The resistance within the cylindrical channel is modified according to

$$\mathcal{R}_{\text{ch}} = \frac{k_B T}{D}\frac{1}{2n_s^{\text{ch}}}\frac{L}{\pi(R_0^2 - R_i^2)}, \tag{35}$$

with $n_s^{\text{ch}} \equiv \sqrt{n_s^2 + (\frac{\Sigma_w R_0 + \Sigma_i R_i}{R_0^2 - R_i^2})^2}$. In the limit of vanishing bulk salt concentration $n_s \to 0$, it reduces to

$$\mathcal{R}_{\text{ch}} = \frac{k_B T}{e^2 D}\frac{L}{2\pi(\Sigma_w R_0 + \Sigma_i R_i)} \tag{36}$$

and reaches a finite value, in agreement with the experimental observations [27]. In the following, we also examine the conductance for pores of different radii as a function of the salt concentration. Correspondingly, the funnel resistance is modified as

$$\mathcal{R}_{\text{funnel}} = \lim_{|x_R - x_O| \to \infty} \frac{1}{\pi}\int_{x_O}^{x_R} dx \frac{\frac{k_B T}{e^2 D}}{2n_s^*(x)(R^2(x) - R_i^2)}, \tag{37}$$

where x_R is the position of the right boundary of the system. In the following, we illustrate numerically the effect of the DNA intruder on the pore conductance.

3. Applications involving channels of variable section and non-uniform surface charge

In the present calculations, we adopt the physical parameters related to DNA translocation set-ups, as reported in [4], which are $L = 34\,\text{nm}$, $R_0 = 5\,\text{nm}$, $R_{\text{DNA}} = 1.1\,\text{nm}$, $\Sigma_i = -0.61\,\text{nm}^{-2}$ and $\Sigma_w = -0.375\,\text{nm}^{-2}$ with surface charge densities being given in number of charges per unit area, $B_0 = 1$ and the total length of the system is 100 nm. The molarity is varied between 0.2 and 1.2 M, $D = 10^{-9}\,\text{m}^2/s$ is the value of the diffusion constant of the ions [5]. Using these data, we obtained for a 1 M solution, the value $\rho_0 = 1.34\ 10^{-1}\ \Omega\,\text{m}$ for a 1 M solution. In Figure 2, we illustrate the partial density profiles in a channel of non-uniform shape. The presence of two steep regions is due to the surface charge discontinuity at the two ends of the cylindrical

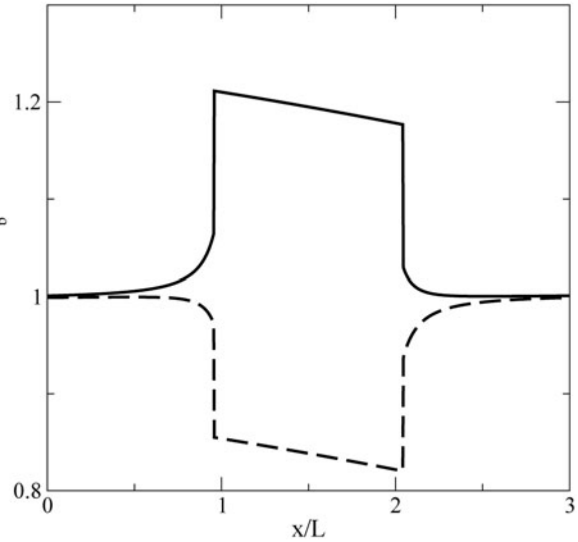

Figure 2. Counter-ion (solid) and co-ion (dashed) density profiles for a funnel pore for a current 4.8 nA. The profile enhancement is due to the surface charge and is very small. The density profiles are non-uniform outside the cylindrical region due to the shape of the funnel. Parameters are $L = 34\,\text{nm}$, $R_0 = 5\,\text{nm}$, $R_{\text{DNA}} = 1.1\,\text{nm}$, $B_0 = 1$, $\Sigma_{\text{DNA}} = -0.61$ and $\Sigma_{\text{wall}} = -0.375$ nm^{-2}.

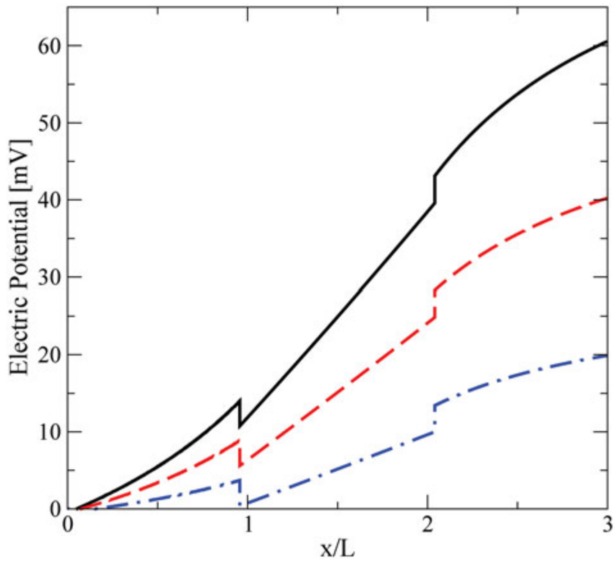

Figure 3. Potential profile for a funnel pore corresponding to three different currents, namely 4.8 nA (solid), 3.2 nA (dashed) and 1.6 nA (dotted-dashed). The position of the potential well corresponds to the region of fixed surface charge. This result is similar to the one observed in the solution of the full PNP problem. Parameters are the same as in Figure 2.

portion. Within the bottleneck, the concentration of co-ions becomes smaller and the co-ions tend to be expelled due to the surface charge. The ion concentration profiles are very sensitive to the applied voltage and at high enough surface charge, the polarisation effect appears to be narrowing.

In Figure 3, we display the potential profile for a funnel pore. The well corresponds to the region where the system is narrower and there is a fixed surface charge. The observed jump is the result of the LEN condition and the discontinuity in the global surface charge. It is the same kind of discontinuity that appears in the treatments of nanofluidic diodes based on the Donnan method [26].

In the case of rather diluted solutions the Debye length cannot be assumed to be small and one has to consider the solution of the Poisson equation, which was avoided by the LEN approximation. Such a solution can be computed by a successive over-relaxation method [30]. Alternatively, one may seek for simple geometries Green's function of the Poisson–Boltzmann problem associated with the linearised Equation (12). However, the general trend is well reproduced even by the LEN, which on the other hand cannot capture the smooth behaviour of the full solution of the Poisson equation.

In Figure 4, we display the *I*–*V* characteristic curve for different molarities. The figure shows that the pore resistance increases with decreasing concentration due to the reduction of the charge carriers. On the other hand, at very low concentrations as illustrated in Figure 5, the conductance does not vanish for pores sufficiently small. In fact, the presence of the surface charge in the narrow

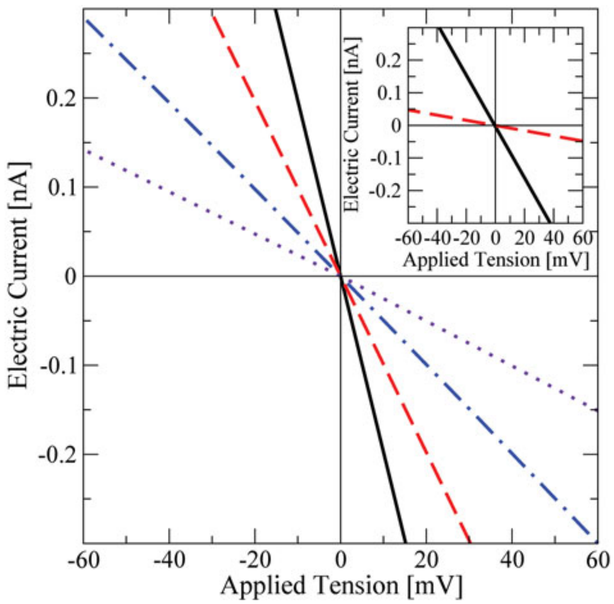

Figure 4. *I*–*V* characteristic curve for different molarities, given by 2×10^{-3} (solid), 10^{-3} (dashed), 5×10^{-4} (dotted-dashed) and 10^{-4} M (dotted line). The resistance increases with decreasing concentration. The remaining parameters are the same as in Figure 2. Inset: *I*–*V* characteristic curve for the funnel with (solid line) and without surface charge (dashed line) in the channel. The resistance is higher without surface charge and the behaviour is linear, and the presence of the surface charge only modifies the resistance.

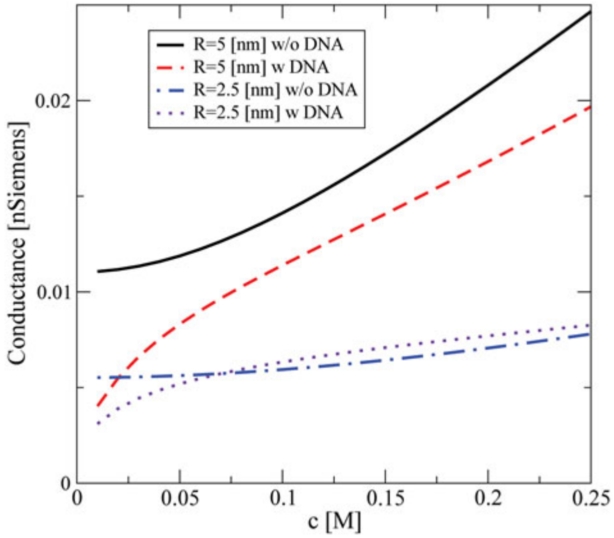

Figure 5. Absolute conductance vs. salt concentration. For vanishing salt concentrations, the conductance of the cylindrical pore reaches a finite value, whereas the conductance of the funnel section vanishes. Parameters are $L = 34$ nm, $R_{\mathrm{DNA}} = 1.1$ nm, $\Sigma_{\mathrm{DNA}} = -0.61\,\mathrm{nm}^{-2}$ and $\Sigma_{\mathrm{wall}} = -0.375\,\mathrm{nm}^{-2}$. The different curves correspond to values of the pore radii $R_0 = 5$ nm and $R_0 = 2.5$ nm as indicated in the box legend. Notice that in the case of the narrower channel the conductance in the presence of the intruder becomes larger than without the intruder, due to the higher effective surface charge.

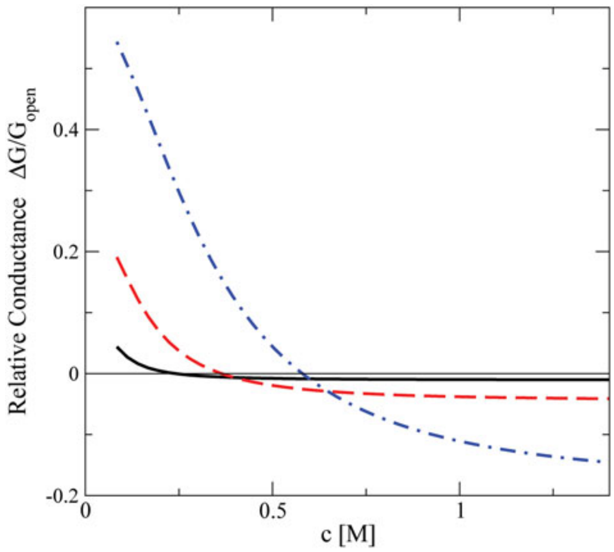

Figure 6. Relative conductance vs. salt concentration in moles. The relative difference between the conductance with the DNA and without intruder but with charge $\Delta G \equiv (G_{\mathrm{DNA}} - G_{\mathrm{open}})/G_{\mathrm{open}}$ is plotted. Parameters are $L = 34\,\mathrm{nm}$, $R_{\mathrm{DNA}} = 1.1\,\mathrm{nm}$, $\Sigma_{\mathrm{DNA}} = -0.61\,\mathrm{nm}^{-2}$, $\Sigma_{\mathrm{wall}} = -0.375\,\mathrm{nm}^{-2}$. The different curves correspond to different values of the pore radii: $R_0 = 2.5\,\mathrm{nm}$ (dot-dashed), $R_0 = 5\,\mathrm{nm}$ (dashed) and $R_0 = 10\,\mathrm{nm}$ (solid line).

regions determines by the mechanism of electroneutrality, an accumulation of counterions in the same region. These counterions are responsible for the so-called surface conduction phenomenon and give rise to a finite conductivity.

For the double funnel geometry illustrated above, we observe that when the surface charge density exceeds a critical value, the resistance of the pore containing the DNA molecule is lower than the bare resistance of the pore without intruder. Such an increase in the conductance is caused by the tendency of the system to accumulate counterions, in order to screen the negative fixed surface charges, thus enhancing the number of charge carriers. Eventually as the surface to volume ratio of the channel increases, such an effect beats the steric hindrance, and the value of the conductance in the presence of the DNA intruder is higher than without the DNA intruder, so that the ratio,

$$\Delta G \equiv \frac{G_{\mathrm{DNA}} - G_{\mathrm{open}}}{G_{\mathrm{open}}}$$

changes sign as shown in Figure 6. Qualitatively the shape of the curve agrees with the experimental ones [27] and we observe a crossover at molarities, which depend on the radius of the pore. Since the Debye length for the present system ranges from 0.3 nm to 1 nm for 1 M and 10^{-1} M solutions, respectively, our approximations hold. The same type of crossover is also evident in Figure 5 for the smaller pore (2.5 nm), but not for the larger.

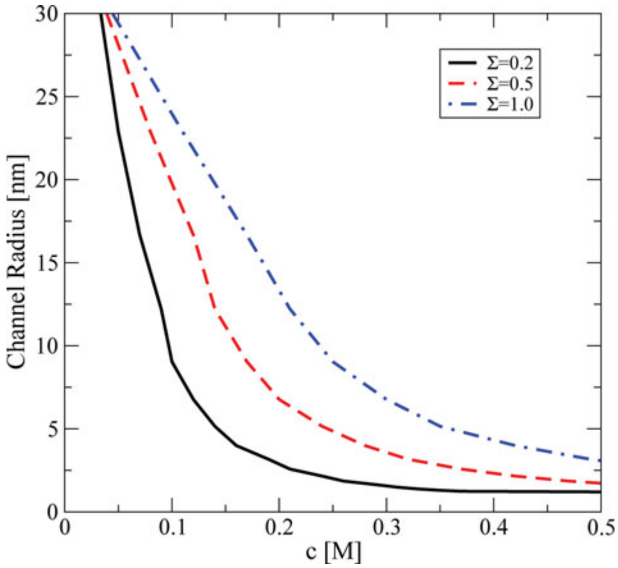

Figure 7. Phase diagram representing the radius at which the difference between the conductance of the open pore and that of the pore with DNA changes sign as a function of the concentration of the electrolyte. Below each of the curves the conduction is enhanced whereas above it is hindered. The three curves are obtained for three different choices of the charge of the intruder and walls, that is by multiplying $\Sigma_{\mathrm{DNA}} = -0.61\,\mathrm{nm}^{-2}$, $\Sigma_{\mathrm{wall}} = -0.375\,\mathrm{nm}^{-2}$ by the factor α 0.2 (solid) , 0.5 (dashed) and 1 (dot-dashed). The enhanced region shrinks if the surface charge decreases.

Finally, in Figure 7, we summarise the observations by presenting a 'phase diagram' using the plane having the concentration and the pore radius as coordinates. The three curves correspond to different values of the total surface charge in the channel. Each curve separates a region where the conductance of the pore is enhanced with respect to the conductance of the pore without a DNA molecule from a region where the current is depleted. Such a diagram was also studied for a straight uniformly charged cylinder by means of a Smoluchowski–Poisson–Boltzmann approach [31] in a situation where the surface charge was much smaller and thus the electro-osmotic effect dominant.

4. Conclusions

The goal of the present paper was to assess the modulation of ionic currents in a charged nanopore with and without the presence of a DNA molecule in the pore. Such set-up is typically realised in experiments involving DNA translocation in solid-state pores. Once a fully stretched DNA molecule threads in the pore, data have revealed either an enhancement or a (partial) blockage of ionic current. For this purpose, we have elaborated an analytical method to determine the charge distribution under transport conditions and the characteristic curves. Such a model relies on the homogenisation of the electrodiffusive equations and the LEN condition.

The method of homogenisation presented here is general and finds applications in the analysis of charge transport in confined geometries, therefore it is a viable and efficient substitute of more detailed descriptions. In spite of the approximations involved, it offers a valid opportunity to deduce analytically the main physical characteristics of ion transport in channels. In addition, the method can be advantageously employed to precondition the solutions of more computationally demanding methods, such as 3D density functional calculations [32] and Lattice Boltzmann solutions [33].

In the future, we plan to exploit this model to study systems in contact with two reservoirs characterised by different salt concentrations. In this case, the conductivity in the reservoir of higher concentration is larger. Thus as the current flows the potential drop is smaller than the side at low concentration.

Acknowledgements

The authors wish to thank Ignacio Pagonabarraga, Mauro Chinappi, Michele Monteferrante and Valerio Mazzone for insightful discussions.

Funding

UMBM acknowledges the support received from the European Science Foundation (ESF) for the activity entitled ‘Exploring the Physics of Small Devices (EPSD)’ under the grant 3720.

References

[1] L.-J. Cheng and L.J. Guo Chem. Soc. Rev. **39**, 923 (2010).

[2] H. Daiguji, P. Yang, and A. Majumdar, Nano Lett. **4**, 137 (2004).

[3] I. Vlassiouk, S. Smirnov, and Z. Siwy, Nano Lett. **8**, 1978 (2008).

[4] S.W. Kowalczyk, A.Y. Grosberg, Y. Rabin, and C. Dekker, Nanotechnology **22**, 315101 (2011).

[5] M. Wanunu, J. Sutin, and A. Meller, Nano Lett. **9**, 3498 (2009).

[6] H.-C. Chang, G. Yossifon, and E.A. Demekhin, Annu. Rev. Fluid Mech. **44**, 401 (2012).

[7] W.E. Morf, Analyt. Chem. **49**, 810 (1977).

[8] M. Jacobs, *Diffusion Processes* (Springer-Verlag, New York, 1967).

[9] R. Zwanzig, J. Phys. Chem. **96**, 3926 (1992).

[10] D. Reguera and J. Rubi, Phys. Rev. E **64**, 061106 (2001).

[11] P. Kalinay and J. Percus, Phys. Rev. E: Stat. Nonlin. Soft Matter Phys. **74**, 041203 (2006).

[12] I. Kosińska, I. Goychuk, M. Kostur, G. Schmid, and P. Hänggi, Phys. Rev. E **77**, 031131 (2008).

[13] A. Berezhkovskii, M. Pustovoit, and S. Bezrukov, J. Chem. Phys. **126**, 134706 (2007).

[14] C.L. Gardner, W. Nonner, and R.S. Eisenberg, J. Comput. Electron. **3**, 25 (2004).

[15] S. Melchionna and U.M.B. Marconi, EuroPhys. Lett. **95**, 44002 (2011).

[16] Antonio Ramos, editor, *Electrokinetics and Electrohydrodynamics in Microsystems*, CISM International Centre for Mechanical Sciences (Springer, Vienna-New York, 2011).

[17] D. Constantin and Z.S. Siwy, Phys. Rev. E **76**, 041202 (2007).

[18] J. Cervera, B. Schiedt, and P. Ramirez, EuroPhys. Lett. **71**, 35 (2005).

[19] J. Cervera, B. Schiedt, R. Neumann, S. Mafé, and P. Ramírez, J. Chem. Phys. **124**, 104706 (2006).

[20] U.M.B. Marconi, S. Melchionna, and I. Pagonabarraga, J. Chem. Phys. **138**, 244107 (2013).

[21] S. Reboux, F. Capuani, N. Gonzalez-Segredo, and D. Frenkel, J. Chem. Theory Comput. **2**, 495 (2006).

[22] D. Gillespie, W. Nonner, and R.S. Eisenberg, J. Phys. Condens. Matter **14**, 12129 (2002).

[23] J.W. Perram and P.J. Stiles, Phys. Chem. Chem. Phys. **8**, 4200 (2006).

[24] D.E. Goldman, J. Gen. Physiol. **27**, 37 (1943).

[25] K. Kontturi, L. Murtomäki, and J.A. Manzanares, *Ionic Transport Processes: In Electrochemistry and Membrane Science* (Oxford University Press, Oxford, 2008).

[26] L. Bocquet and E. Charlaix, Chem. Soc. Rev. **39**, 1073 (2010).

[27] R.M. Smeets, U.F. Keyser, D. Krapf, M.-Y. Wu, N.H. Dekker, and C. Dekker, Nano Lett. **6**, 89 (2006).

[28] B. Hille, *Ionic Channels of Excitable Membranes* (Sinauer Associates Inc., Sunderland, MA, 1984), Vol. 174.

[29] J.E. Hall, J. Gen. Physiol. **66**, 531 (1975).

[30] W.H. Press, B.P. Flannery, S.A. Teukolsky, and W.T. Vetterling, *Numerical Recipes in FORTRAN 77: The Art of Scientific Computing (Volume 1 of Fortran Numerical Recipes)* (Cambridge University Press, New York, 1992), Vol. 1.

[31] B. Luan and G. Stolovitzky, Nanotechnology **24**, 195702 (2013).

[32] U.M.B. Marconi and S. Melchionna, J. Chem. Phys. **126**, 184109 (2007).

[33] U.M.B. Marconi and S. Melchionna, Langmuir **28**, 13727 (2012).